11^{th} International Conference on Fracture Mechanics of Concrete and Concrete Structures
FraMCoS-11
J. M. Chandra Kishen, A. Ramaswamy, S. Ray and R. Vidyasagar (Eds)
https://doi.org/10.21012/FC11.092391

INVESTIGATION ON THE INFLUENCE OF INTERFACIAL TRANSITION ZONE (ITZ) ON CONCRETE CRACKING USING ACOUSTIC EMISSION TECHNIQUE

DINESH K. SAMAL*, SONALISA RAY† AND HEMALATHA THIYAGARAJAN‡

*Indian Institute of Technology Roorkee (IITR)
Roorkee, India
e-mail: dsamal@ce.iitr.ac.in

†Indian Institute of Technology Roorkee (IITR)
Roorkee, India
e-mail: sonarfce@iitr.ac.in

‡CSIR-Structural Engineering Research Centre
Chennai, India
e-mail: hemalatha@serc.res.in

Key words: Acoustic Emission, Interfacial Transition Zone, Composites, Durability

Abstract. The interfacial transition zone (ITZ) is the region between the aggregate and the cement paste in concrete, where the two materials come into contact and interact. It is a critical region in concrete as it represents the gradual transition in composition, microstructure, and properties from those of the aggregate to those of the cement paste. The properties of the ITZ are influenced by various factors, including the properties of the aggregate, curing conditions, and water-cement ratio. The interfacial transition zone plays a crucial role in the behavior of concrete structures due to its unique composition and properties. This study focuses on investigating the cracking mechanisms in concrete with different water-cement ratios using the acoustic emission technique and to evaluate the influence of ITZ volume fraction on cracking in concrete.

Notched plain concrete beam specimens of dimensions 700 mm x 150 mm x 80 mm were cast with water-cement ratios varying between 0.3-0.5. Aggregates with a nominal maximum size of 12.5 mm have been used for this study. Experiments have been performed in a closed-loop servo-controlled Controls testing machine with a load cell of 10 kN capacity under centre point monotonic loading. The beams are tested under crack mouth opening displacement (CMOD) control at a rate of 0.5 µm/s. Acoustic emission technique was used to identify and monitor the development of cracks in the specimens, and the ITZ volume fraction was determined using the mathematical model proposed by authors. Correlations between acoustic emission parameters and ITZ volume fraction were analyzed to describe the effect of ITZ volume fraction on concrete damage.

Based on the present study, it has been observed that the volume fraction of ITZ has a significant influence on concrete fracture. This study provides insights into the behavior of the interfacial transition zone and its effect on concrete damage and cracking process. Damage in concrete, due to the cracking has been studied with the help of statistical analysis of critical AE parameters such as rise time, average frequency, reverberation frequency etc. The acoustic emission parameters, including counts, absolute energy, and amplitude, were found to be positively correlated. The effect of ITZ volume fraction on the damage and fracture has been studied through b-value analysis using the generalised logistic equation. Inter-event time distribution analysis has been performed to evaluate the

burstiness of AE waveforms and get insights into cracking mechanisms of concrete with varying ITZ volume fraction. The results from the study shows the difference in role of ITZ in both normal and high strength concrete. The study also highlights deviations in micro-cracking and macro-cracking patterns along with the crack classification in normal and high strength concrete.

1 INTRODUCTION

Concrete, being one of the most widely used construction materials, plays a crucial role in shaping modern infrastructure. However, despite its exceptional compressive strength, concrete exhibits inherent weaknesses in tensile strength and crack resistance. One of the primary factors contributing to concrete's susceptibility to cracking is the interfacial transition zone [10], which is the region where aggregates and cement paste meet. The damage in concrete can be characterised with the help of fracture process zone (FPZ) which is a zone of micro-cracks ahead of the notch tip [7, 12, 13]. The micro-cracks in the concrete composite are highly influenced by the interfacial transition zone. Understanding the behavior and impact of the ITZ on concrete cracking is essential for ensuring the durability and long-term performance of concrete structures [7, 11]. In the present research, notched concrete specimens with different w/c ratios are subjected to center point loading. The study examines the influence of ITZ on damage and cracking mechanisms, utilizing AE parameters, inter-event time distribution analysis, and b-value analysis.

2 EXPERIMENTAL PROGRAM

2.1 Materials and test specimen

Plain concrete mixes were prepared using locally available raw materials. The mixes included Grade-43 ordinary Portland cement, sand, and coarse aggregates with a maximum size of $12.5\,\mathrm{mm}$, along with a polycarboxylic ether based high range water reducing agent. The fine and coarse aggregates had specific gravities of 2.7 and 2.65, respectively. The design of the concrete mix has been done by following the procedure specified by IS 10262-2009 ([3]). The concrete mix S-3 was designed for a target strength of 45 MPa with a w/c ratio of 0.4. For varying compressive strength, five different water-cement ratios were considered while keeping other mix parameters constant. To represent different w/c ratios, the mixes were labeled as S-1, S-2, S-4, and S-5 for w/c ratios of 0.3, 0.35, 0.45, and 0.5, respectively.
For each category, six concrete cubes of 150 mm length were cast to measure the compressive strength at 28 days following IS:516-1959 ([2]). Additionally, ten concrete cylinders of dimensions 150 $\times$ 300 mm were tested from each category to predict the split tensile strength and modulus of elasticity, following IS:516-1959 ([2]). The quantities of various ingredients used in the concrete mix were presented in Table 2. The volume fraction of ITZ has been determined with the help of an analytical formula given by the authors [1] and is as follows:

$$f_{ITZ} = \frac{(g)^{0.92} * (w/c)^{0.83}}{14.88 * (D_{min})^{0.34} * (D_{max})^{0.49}} \quad (1)$$

Where f_{ITZ}, g, w/c, D_{min} & D_{max} are the volume fraction of ITZ, aggregate fraction, w/c-ratio, minimum and maximum size of aggregate respectively.

Table 1: Mix details

Specimens	w/c	Cement ($\mathrm{kg\,m^{-3}}$)	Fine Aggregate ($\mathrm{kg\,m^{-3}}$)	Coarse Aggregate ($\mathrm{kg\,m^{-3}}$)	Water ($\mathrm{kg\,m^{-3}}$)	Superplasticizer ($\mathrm{L\,m^{-3}}$)
S-1	0.3	413	657	1162	123.9	11.2
S-2	0.35	413	657	1162	144.5	8.3
S-3	0.4	413	657	1162	165.2	-
S-4	0.45	413	657	1162	185.8	-
S-5	0.5	413	657	1162	206.5	-

The mechanical properties such as compressive strength, split tensile strength and modulus of elasticity have been evaluated and are presented in Table 2.

Table 2: Hardened properties of the specimens

Specimens	Compressive strength (MPa)	Tensile strength (MPa)	Modulus of Elasticity (MPa)
S-1	65.9 (2.5)	3.7 (0.4)	40132.7 (362.8)
S-2	53.08 (3.1)	3.3 (0.2)	39299.6 (764.8)
S-3	47.9 (2.4)	3.2 (0.2)	34965.2 (800.8)
S-4	38.7 (2.3)	2.7 (0.3)	35638.9 (752.8)
S-5	31.2 (3.7)	2.5 (0.4)	35265.5 (401.7)
∗ Number in brackets indicate the standard deviations			

The experimental parameters, such as specimen size, notch-to-depth ratio, and CMOD rate, adhered to the recommendations from RILEM TC50 - FMC ([4]). While a single sensor detected events in stressed concrete, multiple sensors were utilized and distributed across the object's surface. This ensured that different sensors captured various signal characteristics for the same AE event. Ideally, each area of interest should be within the acoustic range of at least three sensors during the sensor setup [7]. Commonly, a pattern of interlocking triangles or rectangles was employed for sensor placement. Additionally, the maximum inter-sensor spacing was limited to 0.45 m ([5]).
For flexural testing under center-point loading, ten concrete beam specimens were cast for each concrete mix type, with dimensions of 700×150×80 mm (L×D×B). During casting, a thin steel plate was inserted to create a consistent notch-to-depth ratio of 0.2 with a width of 3 mm for all specimens. The geometric details of the beam were presented through a schematic representation in Figure 1.

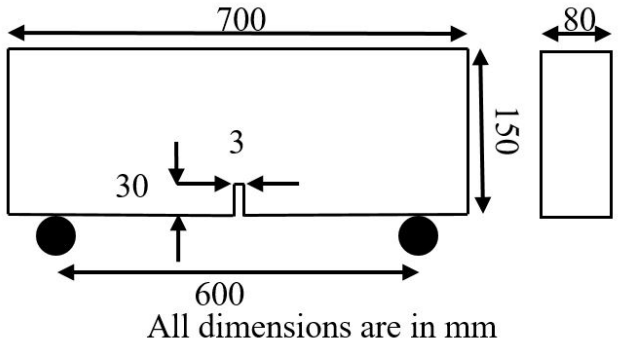

Figure 1: Specifications for the beam specimens.

2.2 Experimental setup

During the center-point bending tests, the beam specimens underwent constant crack mouth opening displacement (CMOD) of 0.5 μm/sec using an MTS-hydraulic system. To measure the crack mouth opening displacement accurately, a clip gauge was positioned at the bottom of the beam.
For recording acoustic emissions during the test, a Digital Sensor-based acoustic multi-channel monitoring system called POWER-PAC, manufactured by the Physical Acoustic Corporation (PAC), was utilized. The system incorporated six sensors, strategically located on both the front and back of the specimens as depicted in Figure 2. These sensors were of the R6α resonant type and were securely attached to the beam surface using grease couplant and fastened with tape. To maintain a high signal-noise ratio, a fixed threshold of 40 dB was employed for detecting acoustic emissions.

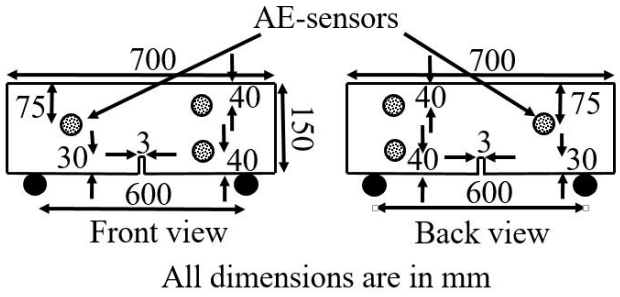

Figure 2: Arrangement of acoustic emission sensors.

2.3 Basic principles of the acoustic emission technique.

The acoustic emission method relies on the generation of acoustic waves during internal deformations like micro-crack formation and grain dislocation in materials. These elastic, transient waves are captured by transducers, preamplified, and then transmitted to detection and measurement systems. The layout of a typical AE system has been presented in Figure 3.

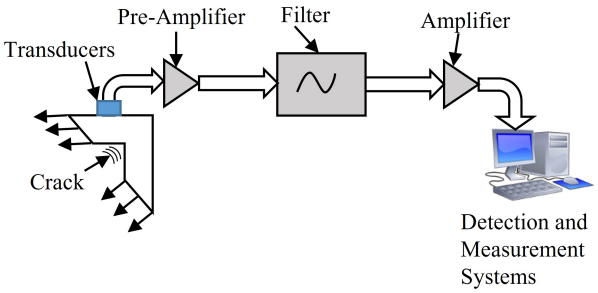

Figure 3: A standard acoustic emission setup.

There are two main types of acoustic emissions based on their source: primary and secondary emissions. Primary emissions originate directly from the material, while secondary emissions come from sources outside the material. These emissions include various waves with different velocities and orientations that propagate through the medium. During their propagation, they undergo changes caused by phenomena like diffraction, dispersion, scattering, reflection from medium boundaries, attenuation, and interaction with reflected waves.

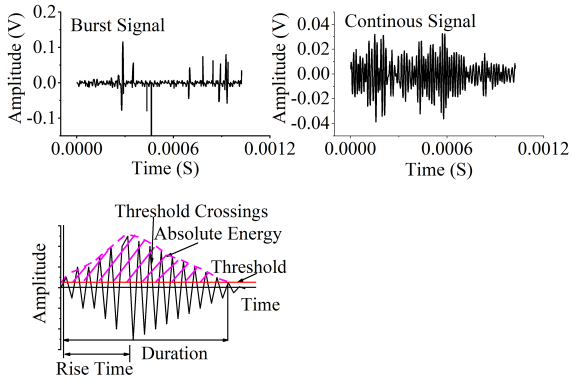

Figure 4: Acoustic emissions parameters.

Acoustically speaking, there are two types of emissions: burst and continuous. Burst emissions are discrete signals arising from individual events within the material, while continuous emissions are sustained signals from overlapping or ongoing events from one or more sources. The both types of acoustic emissions along with various AE parameters has been presented in Figure 4 and defined below.

- Event: It is local deformation in the material giving rise to stress waves.
- Hit: An individual acoustic emission signal detected by a single sensor.
- Amplitude: It is the peak amplitude of the Acoustic emission wave between the first and last crossing and is measured in decibels (dB).
- Threshold: The value of amplitude (in dB) that should be removed from the analysis as background noise.
- Counts: Number of threshold crossings in a single hit.
- Duration: Time taken between first threshold crossing and the last threshold crossing in a single hit.
- Rise-time: It is the time taken to reach maximum peak amplitude measured from the first threshold crossing.
- Acoustic emission energy: AE energy is the area under the envelope of amplitude-time curve above the threshold.
- Peak frequency: The peak frequency refers to the specific point in the power spectrum where the highest magnitude is observed. To obtain the power spectrum of the associated hit's waveform, a real-time Fast Fourier Transform (FFT) is applied to the waveform.
- Frequency centroid: Frequency centroid is the first moment of inertia of the power spectrum and is calculated as follows:

$$\text{Frequency centroid} = \frac{\sum m_i * f_i}{\sum m_i} \quad (2)$$

where m_i and f_i are the magnitude and frequency of the i_{th} bin of the power spectrum respectively.

- Average frequency: Average frequency is the frequency of the entire AE waveform between the first threshold crossing and last threshold crossing and can be calculated as follows:

$$\text{Average frequency} = \frac{\text{Counts}}{\text{Duration}} \quad (3)$$

- Initiation frequency: The initiation frequency can be seen as the rise time frequency and represents the average frequency of the AE waveform from the first threshold crossing to the peak. Initiation frequency can be calculated as:

$$\text{Initiation frequency} = \frac{\text{Counts to peak}}{\text{Rise time}} \quad (4)$$

- Reverberation frequency: The reverberation frequency can be considered as the ring-down frequency, representing the average frequency occurring after the peak of the AE waveform. Reverberation frequency can be calculated as:

$$\text{Reverberation frequency} = \frac{\text{Counts-Counts to peak}}{\text{Duration-Rise time}} \quad (5)$$

3 EVALUATION OF ACOUSTIC EMISSION RESULTS

3.1 Statistical analysis of AE parameters

AE parameters such as rise time, absolute energy, initiation frequency, reverberation frequency and average frequency have a highly skewed distribution. Therefore, taking logarithm can approximate a normal (Gaussian) distribution for those parameters, which is often desirable for various kind of statistical analysis. Figure 5 presents a typical correlation plot of various AE parameters such as rise time, count, absolute energy, peak frequency, frequency centroid, initiation frequency, reverberation frequency, average frequency and amplitude. It can be observed that the absolute energy, amplitude and counts of an AE waveform share a high positive correlation. It is quite obvious that initiation frequency is inversely related to rise time of the associated hit which can also be observed through the correlation plot. It can also be observed that the frequency centroid of an AE waveform is negatively correlated with absolute energy.

Figure 6 illustrates the relationship between the average rise angle ($\approx \frac{\text{Rise time}}{\text{Amplitude}}$) of AE hits and the volume fraction of ITZ. It can be seen that the average rise angle exhibits a general upward trend as the volume fraction of ITZ increases. The higher RA values indicate the formation of a larger number of shear cracks, attributed to the increased probability of debonding at the interface with a higher volume fraction of ITZ. It can also be observed that there is a decrease in the rise angle when the w/c ratio changes from 0.35 to 0.4. This could be attributed to the deviation in the fracture process of normal and high strength concrete wherein, the role of ITZ diminishes in high strength concrete.

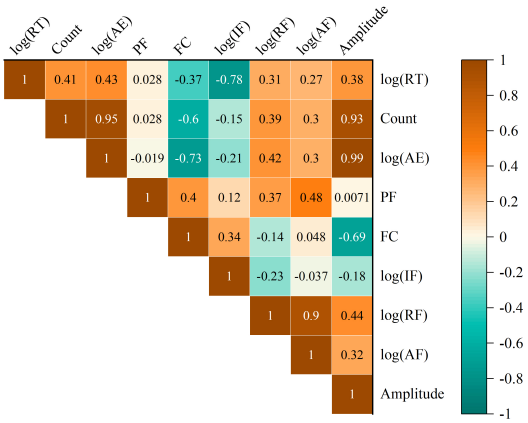

Figure 5: Typical correlation plot between various AE parameters (Here, RT = rise time, AE = absolute energy, PF = peak frequency, FC = frequency centroid, IF = initiation frequency, RF = reverberation frequency, AF = average frequency).

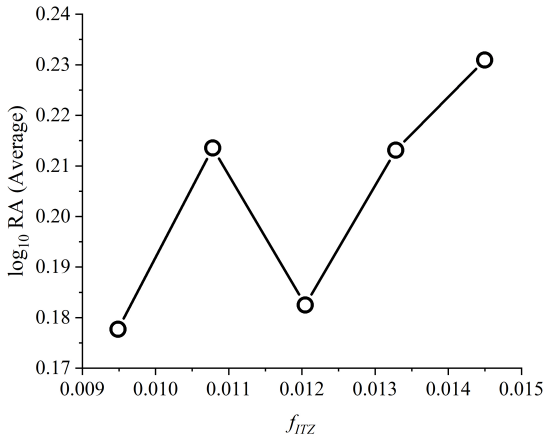

Figure 6: Variation of rise angle with volume fraction of ITZ

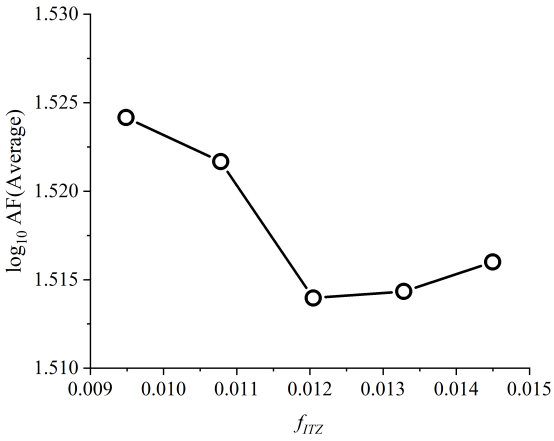

Figure 8: Variation of average frequency with volume fraction of ITZ

Figure 7 shows the variation of mean reverberation frequency across varying volume fractions of ITZ. The mean reverberation frequency is a measure of the time it takes for sound waves to decay in a material after the initial sound source is removed. From Figure 7, it can be observed that reverberation frequency shows a decreasing trend with increasing volume fraction of ITZ. This decline in reverberation frequency indicates a decline in stiffness which can be attributed to the increase in ITZ volume fraction.

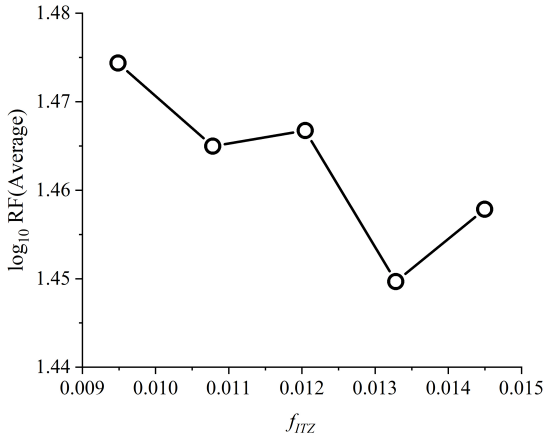

Figure 7: Variation of reverberation frequency with volume fraction of ITZ

The variation of mean average frequency across varying volume fraction of ITZ has been presented in Figure 8. The data clearly shows that the mean average frequency experiences a decline as the volume fraction of ITZ increases up to a certain point, after which it stabilizes and remains constant despite any further increase in the volume fraction of ITZ. Higher mean average frequency in concrete specimens with lower ITZ volume fraction signifies increase in larger number of tensile cracks. This could be attributed to stronger and thinner ITZ in high strength concrete leading to lesser micro-cracks at the interface.

3.2 Inter-event time analysis

Complex systems, such as societies, cells, and natural phenomena, exhibit dynamics characterized by the loosely coordinated activity of multiple components. While progress has been made in studying the underlying networks of these systems, comprehending the governing dynamics has presented greater challenges. Recent developments in monitoring the time-resolved activity of components in various complex systems, such as email communication, web browsing, and gene expression, have introduced fresh avenues for exploration.

A common feature that has been increasingly documented across diverse systems is the phe-

nomenon of burstiness in their activity patterns. Burstiness refers to the presence of significantly enhanced activity levels occurring over short periods, followed by prolonged periods of inactivity. This characteristic has been observed in various systems, including email patterns, earthquakes, and gene expression.

In this section, we aim to explore the significance of burstiness in the fracture process of concrete, using analysis of inter-event time distribution of acoustic emission events. Understanding the burstiness of acoustic emission events during fracture of concrete can provide valuable information about the material's failure mechanisms. By quantifying the magnitude and potential origin of bursty patterns in real materials, we can establish a firmer quantitative basis for studying fracture processes and gaining deeper insights into the underlying dynamics.

Goh and Barabási [9] introduced a parameter called "Burstiness Parameter" to characterise the deviation from a Poisson process with the help of coefficient of variation of inter-event time distribution. Authors defined the burstiness parameter as follows:

$$B = \frac{\frac{\sigma_t}{m_t} - 1}{\frac{\sigma_t}{m_t} - 1} = \frac{\sigma_t - m_t}{\sigma_t + m_t} \tag{6}$$

Where σ_t & m_t are the standard deviation and mean of the inter event time distribution.

In the context of real-world finite signals, the parameter B assumes a value within the limited interval of $(-1, 1)$, and its magnitude is directly related to the signal's burstiness. A value of $B = 1$ indicates the highest level of burstiness in the signal, $B = 0$ represents a neutral state, and $B = 1$ corresponds to a completely regular or periodic signal.

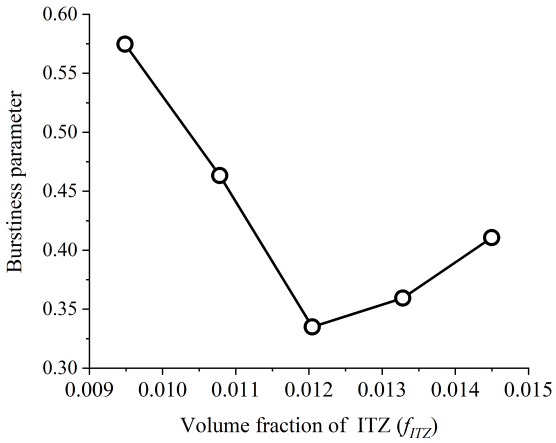

Figure 9: Variation in burstiness parameter with volume fraction of ITZ.

A decreasing burstiness parameter implies that the temporal clustering of AE events is reducing. It could be an indication that the cracks are becoming more distributed and less concentrated in specific regions of the material. An increasing burstiness parameter may imply that certain regions of the material are more susceptible to crack propagation, leading to clusters of AE events in those areas. It can be observed from Figure 9 that the burstiness parameter initially decreases and then starts increasing with the increase in volume fraction of ITZ. The observed differences in the fracture processes of normal and high strength concrete account for these findings. The rise in burstiness parameter with increasing ITZ volume fraction in normal strength concrete suggests that the ITZ is more prone to cracking compared to the aggregate, resulting in heightened localized cracking activity. Conversely, in high strength concrete, the burstiness parameter decreases as the volume fraction of ITZ increases, indicating a more uniform distribution of microcracks throughout the concrete composite, with microcracks developing in both aggregate and ITZ regions.

3.3 b-value analysis utilizing generalised logistic equation

The Gutenberg-Richter (GR) law has been a cornerstone in earthquake statistics for decades

and continues to hold relevance not only in seismology but also in various other fields. It characterizes the frequency-magnitude relation of earthquake events by a power law where the exponent is known as the b-value. showing self-similarity and scaling in seismic events. The b-value near criticality tends to approach a constant value ($b \approx 1$), signifying universality.
The GR law's universality and self-similarity make it potent for comprehending intricate processes during critical transformations. Its self-similarity enables extrapolating larger events from smaller ones. Nonetheless, researchers note deviations in the cumulative frequency distribution (CFD), questioning the oversimplified GR law. To address this, the CFD must incorporate small magnitude events and consider the presence of a large magnitude cut-off and log-concavity.
An approach based on logistic equation proposed by Maslov $et\ al.$ [6] has been proven to be effective in considering the log-concavity and cut-off magnitude of the cumulative frequency distribution as nonlinearities [8]. This two-parameter model considers the nonlinearity of the CFD across the entire magnitude range, incorporating a gentle cut-off for larger magnitudes. This model by Maslov $et\ al.$ [6] is characterised by a unique fractional power-law exponent, indicating that growth of microcracks follow a logistic or sigmoid pattern rather than a power-law. It has been concluded by Burud $et\ al.$ [8] that the b-value derived from the logistic equation demonstrates compliance with damage behavior.

3.3.1 Generalized logistic equation

In their study, Maslov $et\ al.$ [6] introduced a new equation, termed the "generalized logistic equation," to analyze earthquake distribution statistics. A particular form of this equation is given below:

$$P(x) = \frac{Ce^{\frac{-s}{1-\alpha}x^{1-\alpha}}}{1 + Ce^{\frac{-s}{1-\alpha}x^{1-\alpha}}} \quad \text{for } 0 \leq x \leq \infty \quad \text{and} \quad 0 \leq \alpha \leq 1 \tag{7}$$

The Equation 7 is not a perfect cumulative distribution function, but it can be considered an approximation to the CFD when the constant C is sufficiently large [8]. The Parameters α and s of the function $P(x)$ provides an estimate of the number of elements with a size greater than xm, where, x represents the size of an element in a structure, such as the magnitude of earthquakes or the amplitude of acoustic emission events. The function $P(x)$ ranges from $\frac{C}{(1+C)}$ for x = 0 to 0 as x approaches ∞.
Burud et al. [8] showed that for large values of C ($\frac{C}{(1+C)} \approx 1$), the denominator of Equation 7 behaves as a normalizing function. Therefore, to arrive at an expression analogous to the GR law, the denominator of the equation can be removed, and the variable x can be replaced with magnitude m. The resulting equation has been presented as Equation 8. It has also been noted by authors that Equation 8 is a first order approximation of Equation 7.

$$N(m) \quad = Ce^{\frac{-s}{1-\alpha}m^{1-\alpha}} \tag{8}$$

Authors arrived at an expression similar to the GR law by rewriting the Equation 8 in logarithmic form which is as follows:

$$\log_{10}(N(m)) = \log_{10}(C) - \frac{s}{1-\alpha}m^{1-\alpha}\log_{10} e \tag{9}$$

Equation 9 considers the non-linearity in cumulative frequency distribution contrary to the GR law which assumes a linear relation between the magnitude m and the cumulative number of events $N(m)$. Authors [8], considered the parameter α as a penalty on the GR law introduced due to the non linearity of cumulative frequency distribution. The b-value after using the generalised logistic equation to approximate the CFD is as follows:

$$b_{GLE} \quad = \frac{s}{1-\alpha}\log_{10} e \tag{10}$$

The b-value indicates the relative proportion of small to large cracks in the material. Figure 10 presents the variation of mean b-value along with the associated standard deviations across varying volume fraction of ITZ. The comparison reveals that, in general, mean b-values are

higher for normal strength concrete when compared to high strength concrete. Furthermore, it is evident that the mean b-value experiences a reduction as the volume fraction of ITZ increases in both normal and high strength concrete, indicating a greater prevalence of microcracks as the volume fraction of ITZ decreases.

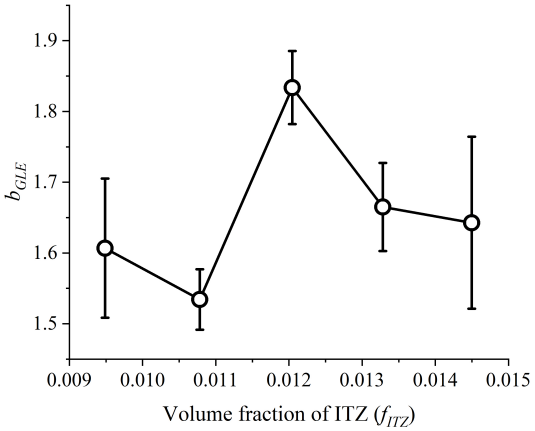

Figure 10: Variation of b-value with the volume fraction of ITZ.

4 CONCLUSIONS

The following conclusions are drawn out of this research work.

- Statistical analysis of Ae parameters revealed the role of ITZ in fracture processes of normal and high strength concrete.
- An increase in the ITZ volume fraction results in a decrease in the stiffness of concrete.
- The presence of a stronger and thinner ITZ in high strength concrete results in a reduced occurrence of micro-cracks at the interface.
- With increasing ITZ volume fraction in normal strength concrete leads to a greater susceptibility to cracking in the ITZ compared to the aggregate, resulting in localized cracking activity.
- With an increase in the ITZ volume fraction in high strength concrete, there is a noticeable shift towards a more uniform distribution of microcracks throughout the material. These microcracks are observed to form in significant numbers in both aggregate and ITZ regions.
- In both normal and high strength concrete, the b-value decreases with an increase in the volume fraction of ITZ, suggesting a higher occurrence of microcracks as the ITZ volume fraction declines.

Acknowledgement

This paper has been assigned the registration number CSIR-SERC-1053/2023

REFERENCES

[1] Samal, D. K. and Ray, S. and Thiyagarajan, H. 2022. Influence of Differential ITZ Thickness around the Aggregate on Properties of Concrete. *Journal of Materials in Civil Engineering* **34(7)**:04022140 .

[2] IS: 516-1959. *Indian Standard Methods of Tests for Strength of Concrete*, Bureau of Indian Standards, New Delhi, India.

[3] IS: 10262-2009. *Indian Standards for Concrete Mix Proportioning Guidelines Specification*, Bureau of Indian Standards, New Delhi, India.

[4] Ohtsu, M. 2010. Recommendations of RILEM TC 212-ACD: Acoustic Emission and Related NDE Techniques for Crack Detection and Damage Evaluation in Concrete: Test Method for Classification of Active Cracks in Concrete Structures by Acoustic Emission. *Materials and Structures* **43(9)**:1177-1181

[5] Polyzos, D. and Papacharalampopoulos, A. and Shiotani, T. and Aggelis, D. G. 2011. Dependence of AE parameters on the propagation distance. *Journal of Acoustic Emission* **29**:57-67

[6] Maslov, L. A. and Chebotarev, V. I. 2017. Modeling Statistics and Kinetics of the Natural Aggregation Structures and Processes with the Solution of Generalized Logistic Equation. *Physica A: Statistical Mechanics and its Applications* **468**:691-697

[7] Samal, D. K. and Ray, S. 2023. An improved understanding on the influence of water-cement ratio and ITZ on fracture mechanisms in concrete. *Magazine of Concrete Research* **75(16)**:847-863

[8] Burud, N. B. and Chandra Kishen, J. M. 2019. Application of Generalized Logistic Equation for b-value Analysis in fracture of plain concrete beams under flexure. *Engineering Fracture Mechanics* **210**:228-246

[9] Goh, K. I. and Barabási, A. L. 2008. Burstiness and Memory in Complex Systems. *Europhysics Letters* **81(4)**:48002

[10] Samal, D. K. and Ray, S. and Thiyagarajan, H. 2020. Effects of water to cement ratio on concrete fracture parameters. In Prakash R.V. et al (eds), *Structural Integrity Assessment: Proceedings of ICONS 2018*; pp. 347-359.

[11] Samal, D. K. and Ray, S. and Thiyagarajan, H. 2020. Effect of interfacial transition zone on fracture energy in concrete. In Pijaudier-Cabot G. et al (eds), *10th International Conference on Fracture Mechanics of Concrete and Concrete Structures FraMCoS-X*; DOI: https://doi.org/10.21012/FC10.235522.

[12] Kumar, B. and Ray, S. 2022. A multi-scale based fracture characterization in concrete under fatigue loading using critical energy dissipation. *International Journal of Fatigue* **165**:107165.

[13] Kumar, B. and Ray, S. 2023. Effects of water to cement ratio on concrete fracture parameters. In Ikotun D.B. et al (eds), *Materials Today: Proceedings*; DOI: https://doi.org/10.1016/j.matpr.2023.04.075